Do vectors point the way to understanding energy transfer in molecular collisions?†

Matthew L. Costen, Sarantos Marinakis and Kenneth G. McKendrick*

Received 30th January 2008
First published as an Advance Article on the web 18th February 2008
DOI: 10.1039/b618070c

This *tutorial review* examines the proposition that vector properties reveal more about the underlying potential energy surfaces controlling the inelastic exchange of energy in intermolecular collisions than conventional scalar measurements. Exciting recent experimental progress is summarized in the form of six selected cases studies. The new information that has been extracted is compared with the predictions of complementary theory. Likely future prospects and promising avenues for further progress are discussed. The treatment should appeal to all those with interests in the forces governing intermolecular interactions, especially in gas-phase collisions.

1. Introduction

1.1 Context and aims of this article

In this article we aim to present a contemporary view of the inelastic transfer of energy in collisions between molecules. In general, this is a ubiquitous process, whose consequences are profound and widespread. It may, for example, promote or prevent molecules from reacting. It may affect their ability to emit or absorb radiation, and hence be exploited as a diagnostic measure reporting on their environment. It is a key factor controlling behaviour at the extremes of the highest temperatures in flames to the lowest currently achievable in specialist cold-molecule experiments.

We focus our attention in particular on collisions where energy is exchanged to or from rotational motion, often abbreviated as RET (rotational energy transfer). This may or may not accompany changes in other internal, vibrational and electronic motions. This choice is connected to our main proposition, that more can potentially be learned about collisional energy transfer from the measurement of vector properties (*e.g.* velocities and angular momenta) than from more conventional and much more studied scalar properties (*e.g.* rotational and vibrational energies). As we set out to show, much of the detailed information is lost if this is not done in a way that is specific to the detailed rotational quantum states before and after the collision. We aim to provide a tutorial summary of exciting progress in this field in the last few years, updating on earlier reviews on related themes.[1–4]

The scope of the systems we will consider is guided by those that are the most important in the main fields of gas-phase chemistry. The most notable are combustion and the atmosphere, but there are also other more specialized fields, such as technological plasmas, astrophysics and 'ultracold' chemistry. The key species that drive the chemistry are small, generally highly reactive molecules, which are often free radicals with open-shell electronic configurations. The case studies we have chosen all involve diatomic molecules of this type, colliding with simple molecular partners selected for either their fundamental or practical interest.

We note in passing that related reactive systems have experienced a "stereodynamic revolution" over the past approximately 15–20 years. The advantages of vector measurements are now very well established there. The interested reader is referred to reviews of this parallel field.[5–7]

School of Engineering and Physical Sciences, Heriot-Watt University, Edinburgh, UK EH14 4AS. E-mail: k.g.mckendrick@hw.ac.uk; Fax: +44-131 451 3180; Tel: +44-131 451 3109

† One of a collection of reviews on the theme of gas kinetics.

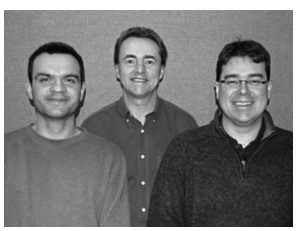

Sarantos Marinakis, Kenneth McKendrick and Matthew Costen (left to right)

Dr S. Marinakis obtained his first degree and MSc in Physical Chemistry from University of Athens working with Prof. J. Samios, and his DPhil from Oxford University supervised by Prof. M. Brouard. He is currently a Research Associate at Heriot-Watt University and has been collaborating with the groups of Profs. F. J. Aoiz (Madrid) and S. Stolte (Amsterdam) on calculations of inelastic collisions.

Kenneth McKendrick has been Professor of Physical Chemistry at Heriot-Watt University since 2000. He was educated at The University of Edinburgh (BSc Hons) and Oxford University (DPhil). He held previous positions as a postdoctoral Research Fellow at Stanford University, CA, USA, and a Lecturer then Senior Lecturer in Chemistry at The University of Edinburgh.

Dr Matt Costen took his MA and DPhil at the University of Oxford under the supervision of Prof. Gus Hancock, followed by post-doctoral research at Brookhaven National Laboratory with Dr G. E. Hall. He returned to the UK to a BP/Royal Society of Edinburgh Research Fellowship at Heriot-Watt University, and is currently a Research Councils UK Academic Fellow.

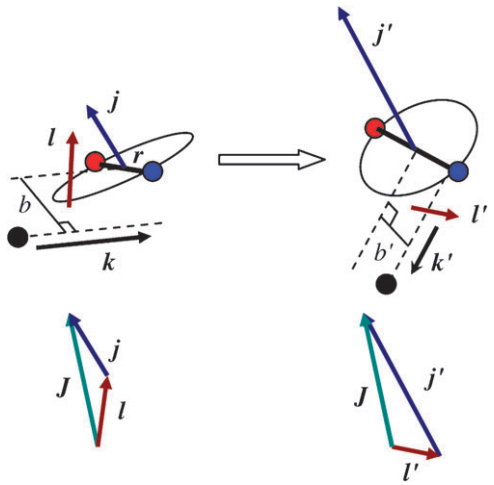

Fig. 1 Key vectors in an atom–diatomic molecule collision.

1.2 Definitions of key vector quantities

The key vectors in a collision between a diatomic molecule and a structureless partner are illustrated in Fig. 1. Relative, linear motion is normally represented by the wavevector, $\boldsymbol{k}$, in the centre-of-mass frame of the collision partners. It is parallel and proportional to the initial relative velocity, $\boldsymbol{v}$. Its magnitude is $k = (2E_T/\mu)^{1/2}/\hbar$, with μ the usual reduced mass of the pair colliding with relative kinetic energy E_T. As is conventional, product attributes are indicated by primes.

Classically, for a closed-shell molecule, the magnitude, j, of the rotational angular momentum measures the speed of rotation. The vector $\boldsymbol{j}$ lies perpendicular to the plane of rotation, which contains the molecular axis, $\boldsymbol{r}$. There is also a so-called orbital angular momentum, $\boldsymbol{l}$, associated with the relative motion of the partners. Its initial magnitude, $l = \mu v b$, is set by v and by the impact parameter, b. This is the (hypothetical) distance of closest approach of the centres-of-mass of the partners if they had continued to travel in straight lines. Conservation of angular momentum requires that the total angular momentum, $\boldsymbol{J}$, is fixed (in magnitude and direction) with $\boldsymbol{J} = \boldsymbol{j} + \boldsymbol{l} = \boldsymbol{j}' + \boldsymbol{l}'$.

We describe below experiments in which the initial distributions of $\boldsymbol{k}$, $\boldsymbol{j}$ (or even $\boldsymbol{r}$) are polarized (*i.e.* not uniformly distributed in space), or the non-random distributions of their polarized counterparts, $\boldsymbol{k}'$ and $\boldsymbol{j}'$, are measured. The correlation between initial and final velocities is the differential cross-section (DCS), proportional to the probability of scattering at a given angle between $\boldsymbol{k}$ and $\boldsymbol{k}'$. The correlations of $\boldsymbol{j}$ or $\boldsymbol{j}'$ with a reference direction can be represented classically as an infinite expansion in a suitable set of basis functions.[7] The reference axis may be either $\boldsymbol{k}$ or $\boldsymbol{k}'$ or, depending on the experiment, a particular direction in the laboratory frame. Provided there is cylindrical symmetry, which will often be the case because of the experimental design, the expansion can be written in Legendre polynomials.

The moments, representing the contributions from terms of each order, K, characterize the distribution. Again because of symmetry constraints, often only the lowest-order moments will be non-zero. The first three are of particular importance, representing, respectively, the population ($K = 0$); the dipolar orientation ($K = 1$), *i.e.* the tendency for molecules to rotate with a particular handedness (clockwise or anti-clockwise); and the quadrupolar alignment ($K = 2$), *i.e.* the tendency for molecules to rotate in a particular plane, regardless of the handedness, as opposed to a perpendicular plane.

In a quantum picture, $\boldsymbol{j}$ is, of course, quantized in direction as well as magnitude. The corresponding spatial distribution is described by the populations of the m_j levels, where m_j is the projection quantum number onto the reference axis. In this representation, an orientation corresponds to a propensity for, say, positive over negative m_j values. A pure alignment has equal populations in the $\pm m_j$ pairs, but favours, say, high values of $|m_j|$ over low $|m_j|$.

As noted above, many of the molecules of interest in this field have open-shell electronic structures, often with unpaired electrons. In these cases, $\boldsymbol{j}$ is not solely made up of rotational angular momentum of the nuclear framework, and contains components of the electronic orbital angular momentum, $\boldsymbol{L}$, and electron spin, $\boldsymbol{S}$. The possible ways in which these couple to form $\boldsymbol{j}$ in diatomics is described by the well known Hund's cases.[8] A recurrent example here is $^2\Pi$ states, which for relatively low values of j are usually best described by Hund's case (a). The levels are split by spin–orbit coupling into well-separated manifolds of fine-structure states (labelled F_1 and F_2). Each level is further split by coupling of the nuclear framework rotation and electronic orbital angular momentum into a pair of Λ-doublets. These are very nearly degenerate, but have distinct symmetry properties (indicated below by e/f parity labels). In the high-j limit, they correspond to the unpaired π-electron density being either in or perpendicular to the plane of rotation.

1.3 The connection between experiment and theory: the potential energy surface

The potential energy surface (PES) represents, by definition, the potential energy of a system as a function of all the nuclear coordinates. The gradients of the PES correspondingly describe the forces. Within the Born–Oppenheimer approximation, the PES contains all there is to know about how a pair of molecules interact. Even when coupling of electronic and nuclear motion cannot be neglected, as happens frequently for the open-shell systems of interest here, it can be treated by considering several PESs and the couplings between them.

Therefore, designing experiments whose results are sensitive to the detailed form of the PES is a central theme of the field of collision dynamics. This provides the primary mechanism for comparison with theory. Theoretical methods are not the main focus of this review, but their predictions are discussed in the context of the experimental results on which we concentrate. In summary, PESs may be generated theoretically in a variety of ways. The ultimate level is a full *ab initio* quantum-mechanical (QM) electronic structure calculation. This aims to be an 'exact' description of a particular system. Semi-empirical or even simpler model surfaces are usually intended to capture the essence of key features of the surface, with the benefits of simplicity and less computational expense.

Similarly, the scattering calculation that predicts the outcome of a particular collision with specified initial conditions

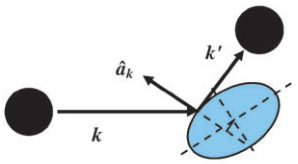

Fig. 2 Hard-sphere + hard-shape model collision.

(E_T, $\boldsymbol{l}$, $\boldsymbol{j}$, *etc.*) can be carried out 'exactly' by (usually time-independent) QM methods. It can also be tackled approximately by classical mechanics, the most rigorous level of which is a quasi-classical trajectory (QCT) calculation. As well as being computationally simpler, an important benefit of simplified model scattering calculations is the qualitative insights that they provide. Many of the key features of inelastic scattering are captured in even the most elementary 'hard-sphere + hard-shape' models. They treat the PES as being infinitely repulsive inside, and zero outside, a given intermolecular distance which is a function of the angle of approach. It is fundamental that no rotational energy can be exchanged if the collision does not exert a torque on the diatomic molecule. In a hard, or 'sudden', collision the forces act along the surface normal of the hard-shape. The capacity to cause a rotational state change is related to the perpendicular distance that the extrapolated normal passes from the centre-of-mass of the molecule, as shown in Fig. 2.

A less obvious extension of this basic idea is the concept of the 'kinematic apse', defined as unit vector $\hat{\boldsymbol{a}}_{\boldsymbol{k}} = (\boldsymbol{k}' - \boldsymbol{k})/|\boldsymbol{k}' - \boldsymbol{k}|$. Because the force imparted in a sudden collision can only act along the surface normal, which for a hard shape coincides with $\hat{\boldsymbol{a}}_{\boldsymbol{k}}$, the angular momentum generated must be perpendicular to $\hat{\boldsymbol{a}}_{\boldsymbol{k}}$. This is the basis of an important propensity rule, that the component of angular momentum along $\hat{\boldsymbol{a}}_{\boldsymbol{k}}$ must be conserved.[3] The apse also appears as a significant reference direction in a number of theoretical treatments, to which we refer further below.

More generally, PESs, which need not be purely repulsive, can usefully be analysed for their ability to cause rotational state-changing collisions by decomposing them into components of different orders in a Legendre expansion. The PES is expressed as an infinite sum:

$$V(R,\theta) = \sum_{\lambda} [V_\lambda(R) P_\lambda(\cos\theta)] \qquad (1)$$

where R is the intermolecular distance, θ is the angle of approach, and P_λ are Legendre polynomials. The lowest order 'spherical', $\lambda = 0$, term can only be responsible for elastic ($\boldsymbol{j}$-conserving) collisions. The 'dipolar', $\lambda = 1$, term is related to the difference between the ends of the diatomic molecule, and can cause rotational state changes for a heteronuclear diatomic. In turn, $\lambda = 2$ distinguishes between the sides and ends of the molecule, and is the lowest term that can induce RET for homonuclear diatomics. Visual inspection of the intermolecular distance-dependence of these terms, as in Fig. 3 for the OH $X^2\Pi$—He and Ar systems,[9,10] allows a qualitative assessment of the strength and range of the potentials governing rotational state-changing collisions.

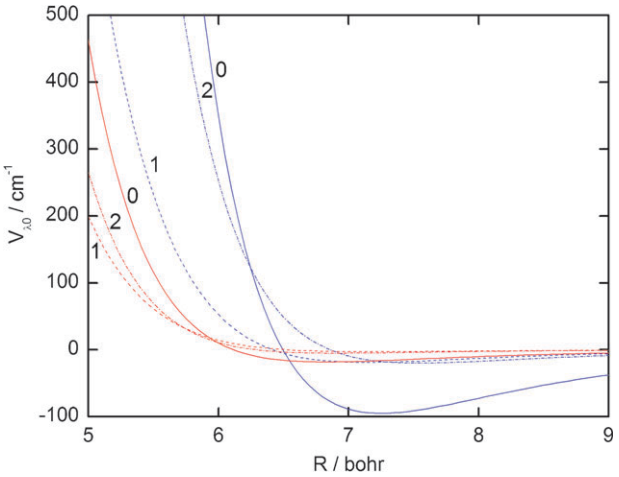

Fig. 3 Lowest Legendre components of order λ, as indicated, of the intermolecular potentials between OH $X^2\Pi$ and He (red) and Ar (blue). [Constructed from data in refs. 9 and 10].

2. Experimental approaches to measuring vector quantities for inelastic scattering

2.1 Conventional experimental approaches

Conventional experimental techniques used to determine the scalar, and to a lesser extent, vector properties of inelastic scattering can be broadly divided into two classes; crossed molecular beams (CMB) and optical–optical double resonance (OODR). Common to all experiments are the need to prepare the molecules in well-defined quantum state distributions with known vector properties, and then to measure those properties after collision under controlled conditions.

The first stage in any experiment is to introduce or, if necessary when not using stable molecules, *e.g.* CO, HCl, I_2, NO, generate the molecule of interest. The other major choice is that of the collider, often a rare gas, although stable diatomic and triatomic colliders (*e.g.* N_2, CO_2) have also been widely studied. These stable molecules are ideally suited to CMB scattering. Molecular beams are formed by expanding the gas (usually seeded in an excess of He or Ar) into a high vacuum.[11] Collisions in the expansion region immediately after the nozzle result in cooling of the internal degrees of freedom of the molecular species and in the transverse translational motion, with the energy redistributed into collective translation away from the nozzle. Rotational cooling of diatomic molecules is very efficient, with temperatures <5 K achieved routinely. Molecular beams thus do provide some state selection, but only in the special sense of confining population to the lowest few rotational states and not complete quantum state control. Their strength is in providing very good initial velocity selection, with a narrow range of speeds in the direction of the beam ($<10\%$ of the centre speed) and a very small angular divergence. The beams of target molecule and collider are crossed, often at 90°, although more sophisticated designs with variable crossing angles allow the collision energy to be tuned. These attributes make CMB ideal for precision measurements of the DCS.

Not all molecules of interest are stable, which is particularly true of radical species important in combustion and atmospheric chemistry, such as OH, CH, NH, CN. In traditional CMB experiments, these molecules were typically prepared using microwave or electric discharges. More recently this has largely been superseded by laser photolysis of suitable precursors. Such photolysis may be coupled to molecular beams,[12] but is more conventionally used as a starting point in optical experiments. These are normally performed with a small fraction of photolytic precursor in an excess of collider gas, a so-called 'bulb' experiment. Photolysis usually produces radicals with very non-Boltzmann state, and anisotropic vector, distributions. The photolytic distribution is thus often allowed to thermalize in collisions with the bath gas to concentrate population in a narrower range of levels. A tunable laser system is then used to excite a fraction of the molecules to a chosen excited electronic and/or vibrational state. A typical pulsed dye laser system will have sufficient resolution to prepare a single isolated rovibronic state of a diatomic or even small polyatomic molecule. Such optical preparation is ideal for scalar studies, but starting from a thermalized velocity distribution is unsuitable for DCS measurement. The optical pumping can however provide orientation or alignment of the rotational angular momentum, which is generally not achieved in molecular beam expansions. Although it has been demonstrated that alignment can be generated in the expansion itself, this is yet to be exploited systematically for collisional energy transfer. We do not discuss it further here.

After a collision some form of probe technique is required to determine the product scalar and vector properties. The classic molecular beam detection method is a rotatable mass spectrometer using electron impact ionization, with the time-of-flight (TOF) of the products from the scattering centre being recorded. This is capable of very high resolution in the product scattering angle, but suffers from the non-selective nature of the ionization, which ionizes all product molecules regardless of internal state. Generally the TOF resolution is not sufficient to observe the DCS for individual product quantum states, except in some exceptional cases.[13] Laser-induced fluorescence (LIF) has been coupled to CMB scattering, with the probe laser beam passing through the molecular beam crossing point.[14] This arrangement does not allow for DCS measurement, but can be used to measure product state propensities.

Product detection in bulb experiments is usually by laser-based spectroscopic methods, hence the designation as OODR as defined above.[2,4,14] In many cases this is by LIF, although Resonance-Enhanced Multi-Photon Ionization (REMPI) and absorption may also be used. Optical excitation of electronically excited states generally leads to fluorescence. Dispersion through a monochromator enables the state-to-state rate constants for transfer in the excited electronic state to be measured. In a very few experiments, the polarization of the fluorescence has been resolved, revealing information on the retention or removal of the prepared angular momentum polarization, a $\boldsymbol{j}$–$\boldsymbol{j}'$ correlation.[15] This is a very challenging experiment, as saturation of the pump step will greatly reduce the prepared polarization, so must be avoided, whilst the polarization optics in the detection system also reduce the signal. A few measurements of $\boldsymbol{j}$–$\boldsymbol{j}'$ correlations have also been made with LIF or REMPI in OODR experiments.[16–18]

These conventional approaches have been widely used to study inelastic collision dynamics. The broad division between CMB and OODR reflects the limitations of each. CMB experiments display limited state resolution but good DCS sensitivity, whilst OODR experiments provide excellent state resolution but are mostly limited to scalar measurements. As we go on to show below, elements from both are needed to make more insightful vector measurements.

2.2 Case studies of novel experimental methods

Recent experimental developments have built on the CMB and OODR methods described above, introducing additional state selection in the preparation and detection stages and extending the range of vector properties measured. Not surprisingly, no single experiment is truly universal. Here we describe six distinct examples that demonstrate the additional information about the PES that can be learnt from different kinds of vector measurements.

2.2.1 Building on the molecular beam approach

Case study 1: Collisions of rotational-state selected NO(X) by velocity-map imaging. The previous section has outlined the principles of CMB scattering, and highlighted the high precision that is in principle possible in the measurement of DCSs using this method. To overcome its principal limitation, a detection method is required that has full quantum-state resolution. One recent approach is to apply REMPI–Velocity Map Imaging (REMPI–VMI).[19] In REMPI, ionization proceeds through a stable resonant intermediate state. This provides spectroscopic state resolution, and ion detection provides the very high sensitivity required to observe the low number densities of scattered products in a CMB experiment. VMI is a recent extension of ion detection in which carefully controlled electric fields forming an ion lens are used in conjunction with a 2-dimensional position sensitive detector. The crucial advantage of VMI is that the location of an ion in the image depends only on its velocity, so that a 2-D image of the motions in the scattering plane is obtained. The REMPI ionization process is also sensitive, through the polarization of the probe laser, to the angular momentum polarization of the scattered molecules. Thus it is possible to determine the highly insightful angular momentum polarization of the scattered products as a function of the scattering angle for individual product states.

Chandler and co-workers have used this technique to study RET in the NO($X^2\Pi$) + Ar system.[20,21] Their experiments start with NO almost exclusively (99%) in the $j = 0.5$ state, with equal populations in the two Λ-doublets. Examples of the ion-images they obtained are shown in Fig. 4. The differences in the ion images for the two orthogonal probe-laser linear polarizations show a strong rotational angular momentum alignment in the product NO, which changes markedly with scattering angle. For small Δj where the product is mostly forward scattered, $\boldsymbol{j}'$ tends to be parallel to $\boldsymbol{v}'$, a 'propellor'-like motion. At larger Δj and more backward scattering there is an increasing tendency for $\boldsymbol{j}'$ to be perpendicular to $\boldsymbol{v}'$, corresponding to 'frisbee' motion. These results were compared to

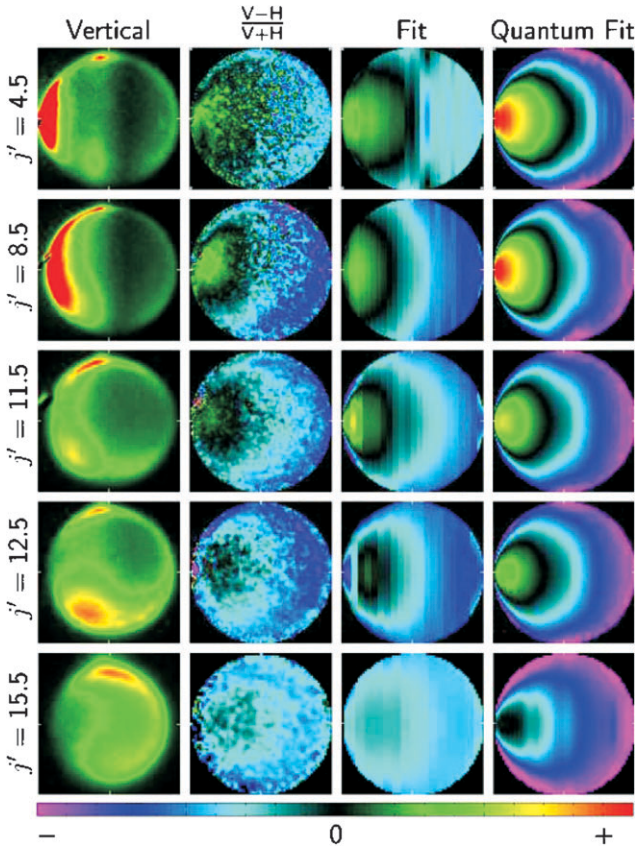

Fig. 4 NO $X^2\Pi_{1/2}(v'' = 0)$ ion images following collision with Ar. First column, images taken with vertical (V) probe laser polarization. Second column, difference images from V and horizontal (H) probe polarizations, (V − H)/(V + H). Third column, least squares fit to difference images, from which the values of the alignment moments have been extracted and fourth column, simulations from QM scattering calculations. (Reprinted from ref. 21 with permission. Copyright 2004 Elsevier).

QM scattering calculations on an *ab initio* PES. The calculations were found to reproduce the general form of the experimental results, but predicted significantly more polarization for the backward scattered products than was observed. As a specific example of the sensitivity of vector properties to the form of the PES, this suggested that the potential required modification in the region of the repulsive wall, probed by these back-scattered trajectories.

Chandler and co-workers went on to make the first ever measurements of scattering-angle resolved orientation.[20] In the same experimental set-up as discussed above, they used circularly polarized probe light to measure the sense of rotation of the scattered NO. They found the beautifully intriguing result that this oscillated between clockwise and counter-clockwise as a function of scattering angle and Δj, as shown in Fig. 5. QM scattering calculations were able to reproduce well the observed orientation and its scattering angle dependence for large Δj. However, at small Δj the choice of PES was found to have a strong effect on the scattering-angle dependence on the sign of the orientation. The authors concluded that this particular measurement, in contrast to that of alignment, is a very sensitive probe of the full range of the PES.

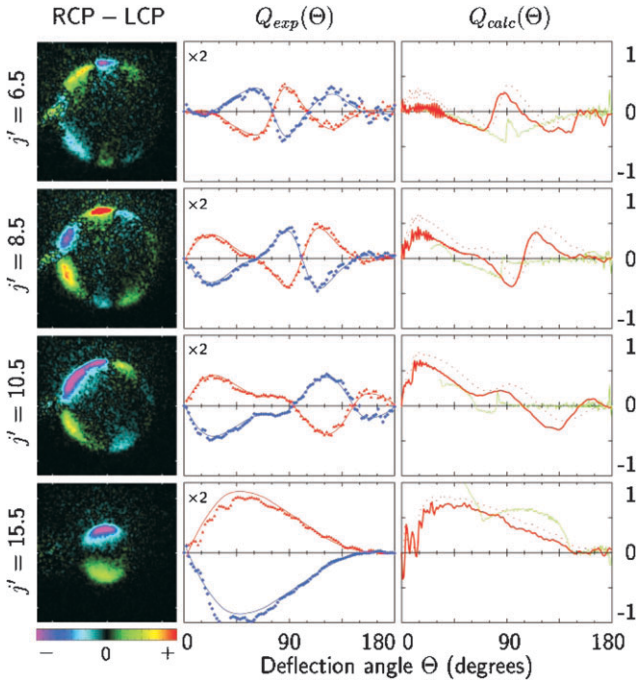

Fig. 5 Left panel, difference of ion images taken with right (RCP) and left (LCP) circularly polarized probe light for NO $X^2\Pi_{1/2}(v'' = 0)$ following collision with Ar. Red indicates clockwise rotation and violet counter-clockwise. Centre panel, extracted scattering angle dependent orientation, $Q_{exp}(\theta)$, from top of image (blue), and bottom of image (red). Right panel, calculated orientations, $Q_{calc}(\theta)$, from: classical rigid ellipsoid model (green), QM scattering calculations on two different PESs (red solid and dotted). (Reprinted from ref. 20 with permission. Copyright 2001 AAAS).

This was evidently better represented by the more recently calculated of the two PESs.

Case study 2: Collisions of NO(X) in single Λ-doublet states by hexapole field selection. In an alternative development of the conventional CMB approach, Stolte and coworkers have refined the level of state-selection by introducing an electrostatic hexapole field. This method has been used successfully to determine the DCS for collisions of a single, isolated Λ-doublet level of NO with He and D_2.[22,23] As described in case study 1 above, cooling in the expansion confines the population effectively into the lowest rotational state NO($j = 0.5$, $\Omega = 0.5$), equally distributed between the very nearly degenerate e and f Λ-doublet levels. The spectroscopic symmetry labels e and f refer to the total space-fixed inversion parity of the electronic wavefunction, exclusive of rotation. These rotationally cold NO molecules entered an electrostatic hexapole selector (see Fig. 6). Because the NO molecules have a dipole moment, $\mu = 0.1732$ D, the Λ-doublets have opposite Stark energies, given by $U = -\varepsilon\mu E|m_j\Omega|/(j(j+1))$, with $\varepsilon = \pm 1$ for the e and f states, respectively.[22] The f states are therefore so-called "low-field seeking" and experience a radial force towards the on-axis region of lowest potential. They follow converging trajectories and can be focused at a point downstream of the selector. Conversely, the e-states diverge and are easily effectively blocked by an aperture. The selected NO($j = 0.5, f$) molecules cross a pulsed molecular beam of the

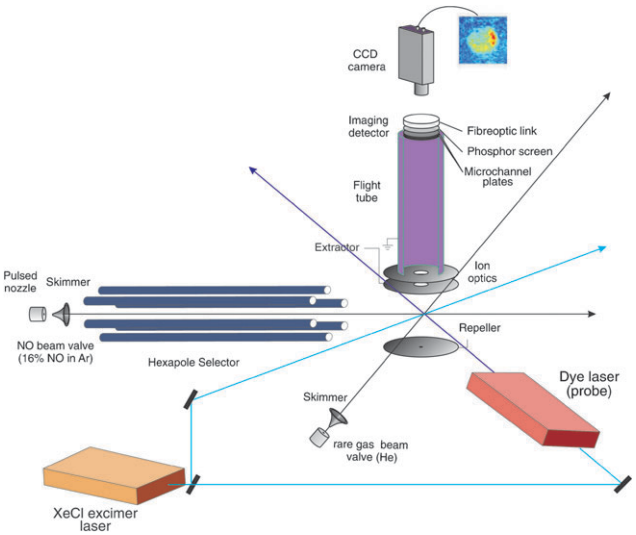

Fig. 6 Schematic crossed beam experimental setup combining hexapole state selection with velocity-map ion imaging detection.

collision partner at 90°. The scattered NO products are detected using the REMPI/VMI technique described above.

The overall behaviour of the fully state-resolved DCSs for collisions with He shown in Fig. 7 is mostly as would intuitively be expected. Forward scattering leads to low Δj transitions and backwards scattering to high Δj. A particular benefit of the additional level of state-selection afforded by the hexapole field is that these studies also provided the first experimental evidence of a new kind of electronic symmetry restriction on the DCS. Starting from the selected single initial Λ-doublet state, differences were found between the DCSs for scattering into the two product Λ-doublets of a given j. It is worth stressing again that the energy differences between Λ-doublets are very small compared to the collision energy or the gap between successive j levels, so this cannot be an energetic effect. Stolte and coworkers realized that apart from an overall scaling factor, the shape of the DCS was the same for scattering into neighbouring final states which had the same space-fixed inversion parity, $p = \varepsilon'(-1)^{j'-0.5}$ and common value of a labelling index, $n = j' - \varepsilon\varepsilon'/2$, as shown in Fig. 7.

To explain these puzzling results, Stolte and coworkers have developed a new, so-called 'Quasi-Quantum Treatment' (QQT) of inelastic scattering.[24,25] In essence, QQT assumes that the direction of the molecular axis, $\boldsymbol{r}$, is fixed during the collision process. The scattering amplitude is expressed in the kinematic apse frame (see section 1.3) as a product of a classical DCS and a phase shift factor. The QQT employs integrals over angular variables (all the possible initial orientations) and, using a hard-shell potential, all of the summation over coupled equations in orbital angular momentum or impact parameters required in conventional treatments is avoided. A significant result is that the shape of the DCS for a $j = 0.5$, $\varepsilon \rightarrow j',\varepsilon'$ transition is predicted to depend on a Legendre polynomial of order $j' - \varepsilon\varepsilon'/2$. Consequently, it is the DCSs for transitions into energetically separated parity pairs associated with successive values of

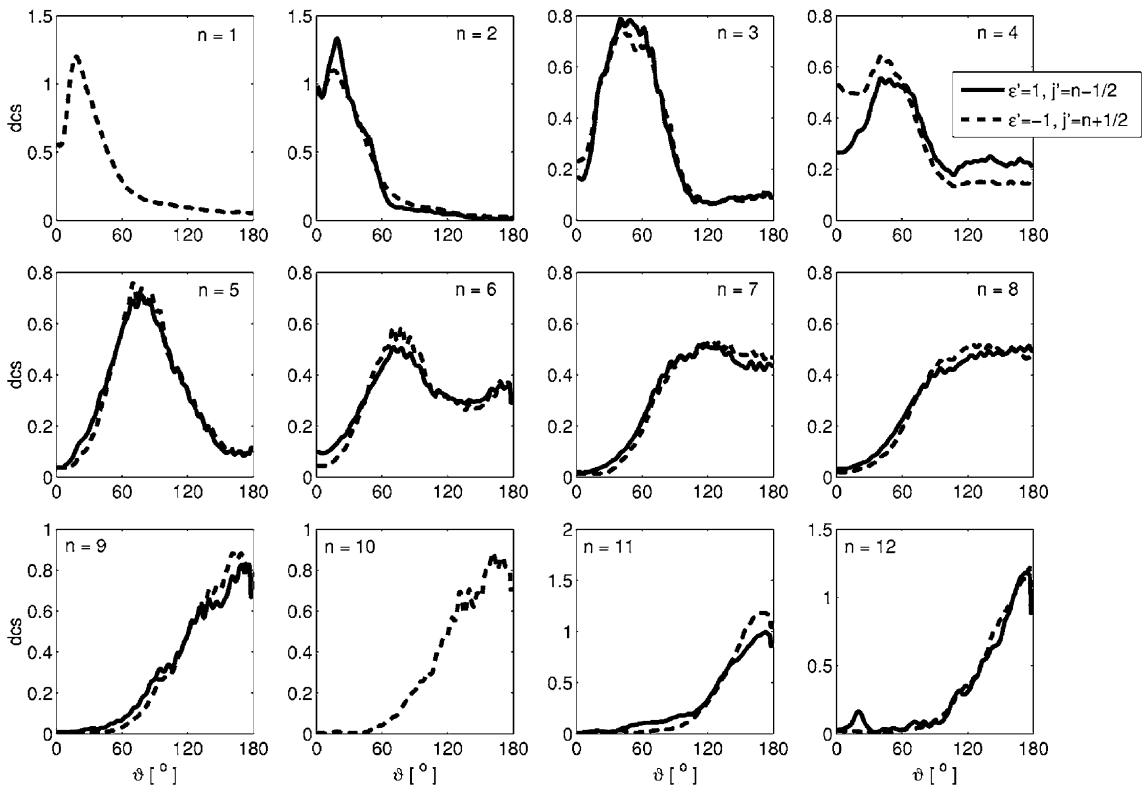

Fig. 7 Fully Λ-doublet state resolved differential cross sections for He + NO($^2\Pi_{1/2}$,$j = 0.5$,f) collisions. Experimental results for spin–orbit conserving transitions into the (j',ε') levels are shown. Normalized differential cross sections are plotted in parity pairs. (Reprinted from ref. 23 with permission. Copyright 2006 American Institute of Physics).

j', rather than of the near-degenerate Λ-doublets, that are determined by the same Legendre polynomial. They should thus have similar shapes, as indeed observed experimentally.

There are some other surprises in the detail beyond those shown in Fig. 7. In particular, the DCS for the $j' = 12.5, e$ state is more sideways than $j' = 11.5, e$. This appears only in the spin–orbit conserving transitions. It is also absent for the corresponding $j' = 12.5, f$ state. This intriguing collapse of the prediction of any classical model has also been verified in exact QM studies,[22] but its physical origin remains a challenge to be explained.

Case study 3: "Steric asymmetry" in collisions of NO(X) by additional electrostatic field selection. The enhanced level of state-selection achieved in case study 2 can be further exploited to examine the effect on the outcome of a collision of orientation of the molecular axis, $\boldsymbol{r}$. This is perhaps the current state-of-the-art of CMB-based techniques. The numerous technical challenges have been overcome in independent studies of NO and OH by the groups of Stolte [26,27] and ter Meulen,[28,29] respectively.

The method requires a linear molecule with non-zero angular momentum, so is well matched to the diatomic radicals of interest here. Its basis is to pass molecules that have already been selected in a specified Λ-doublet state by Stark-induced focusing, as described in case study 2 above,[22,23] adiabatically into a region of homogeneous static electric field placed around the collision zone. The required typical field strengths are around 10 kV cm^{-1}. The sign of $\boldsymbol{E}$, defined as pointing from positive to negative polarity, can be reversed. The field gradient is therefore either parallel or anti-parallel to the initial relative velocity. This has the effect of orienting the molecular axis of the NO($^2\Pi_{1/2}$, $\nu = 0, j = 1/2, f$) or OH($^2\Pi_{1/2}$, $\nu = 0$, $j = 3/2, f$) molecules along the field direction. Either 'end' of the molecule can therefore be presented preferentially to the incoming molecular beam of the collision partner.

The quantum state of the molecule in the electric field is a linear superposition of the field-free parity states (e and f), $|jm_j\Omega E> = 2^{-1/2}[\alpha(E)|jm_j\Omega f> + \beta(E)|jm_j\Omega e>]$ where $\alpha(E)$ and $\beta(E)$ are the mixing coefficients and m_j is the projection of $\boldsymbol{j}$ along $\boldsymbol{E}$.[26] Assuming no long-range collision-induced reorientation, the negatively charged end of a low field seeking molecular rotational state points preferentially towards the negative electrode. This, perhaps intuitively surprising, result can be understood classically. The molecule rotates more slowly and therefore spends more time during the phase of its rotation when it is in the higher energy orientation with the sign of the molecular dipole the same as that of the field. The degree of orientation is given by the mean value of the angle θ between $\boldsymbol{E}$ and the molecular axis. This is predicted by a two-level model, and confirmed previously experimentally, to have a magnitude $\langle\cos\theta(E)\rangle = \alpha(E)\beta(E)\Omega m_j/(j(j+1))$.[26,29]

Using this arrangement, inelastic integral cross-sections for collisions for the two molecular orientations have been measured using saturated LIF. The dependence of the cross sections on the orientation of the incoming molecule is usually expressed by the initial and final-state specific dimensionless steric asymmetry factor, S, which can be written for the example of NO with He as in eqn (2):

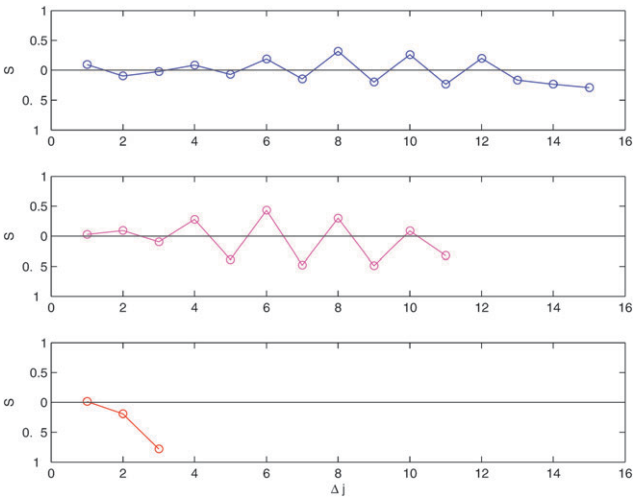

Fig. 8 Experimental steric asymmetry for ($j = 0.5, f \rightarrow j', f$) spin–orbit conserving transitions as a function of Δj for NO + Ar (upper panel), NO + He (middle panel) and OH + Ar (bottom panel) at collision energies of 475, 509 and 746 cm^{-1}, respectively. Note that for Ar + OH, the O-end is regarded as the head of the molecule. (Adapted from ref. 26 with permission. Copyright 2005 Institute of Physics).

$$S(j = 0.5 \rightarrow j',\ \varepsilon') = \left(\frac{\sigma_{\mathrm{He+NO}} - \sigma_{\mathrm{He+ON}}}{\sigma_{\mathrm{He+NO}} + \sigma_{\mathrm{He+ON}}}\right)_{j',\varepsilon'} \qquad (2)$$

For collisions of the OH molecule with Ar,[29] there is a gross dependence of the amount of rotational energy transfer on which end of the OH is struck: the O-end yields relatively low j' levels while the H-end produces higher j' levels. This is in accord with both full QM calculations and with the intuitively predictable results of a simple classical 'ball-and-stick' model. Because the light H-atom is displaced further from the OH centre of mass, it is obviously easier for the collision partner to rotate the OH by hitting the stick (H-end) than the ball (O-end).

In contrast, for collisions of NO with He and Ar,[26,27] the results are not so easily predictable from a classical standpoint, because there is no longer a very large kinematic distinction between the ends of the molecule. The experimental results (see Fig. 8) reveal an interesting oscillatory dependence of S on final rotational state. Collisions with the N-end promote Δj = even transitions preferentially, whereas the O-end favours Δj = odd. Note that the absolute values of S obtained for NO are smaller than for OH. This reflects both a higher degree of initial orientation for OH and also that its charge and mass are more asymmetrically distributed. The measurements of S therefore clearly probe the 'deviation from homonuclearity',[30] *i.e.* the odd Legendre terms in the expansion of the relevant PES.

Perhaps the most striking feature of the Ar + NO results is not the oscillations in S themselves, which are predicted by QM scattering theory and can be rationalized using QQT, but the absolute disagreement in the resulting sign of S between the experiment and the theoretical predictions (both QQT and QM).[25] No explanation has yet been found, opening questions

about the sign of the NO electric dipole moment and possible orientation due to strong laser fields.

Returning to the main theme of this review, the steric asymmetry is found in QM calculations to be dependent mostly on the repulsive part of PES.[30] For example, S values are predicted to be larger for He + NO than for Ar + NO, reflecting the asymmetries in the PESs. Measurements of S, when suitably combined with QQT predictions, can be used to obtain hard-shell potentials even for the more difficult case of molecule–molecule collisions. For the D_2–NO system,[27] the model was sufficiently successful to reproduce the DCS obtained previously.[23] Measurements of S for molecule–molecule collisions are still scarce, but ter Meulen's group has studied OH with several partners including CO, HCl, HBr, HI and N_2.[28] Their interesting results are not yet fully explained. They are thought to require a more accurate description of the PES in the regions of van der Waals wells and, for potentially reactive partners, the regions of the transition states.

2.2.2 Novel spectroscopic approaches

Case study 4: Collisions of rotational-state selected OH(A) by Zeeman quantum beat spectroscopy. In an extension of the traditional optical techniques described above, Brouard and coworkers have developed a new method to give vector information on the collisional decay of rotational angular momentum polarization in electronically excited states. In this so-called Zeeman quantum beat technique, the isotropy of space is deliberately broken by the introduction of a magnetic field. The method has been demonstrated successfully in studies of OH($A^2\Sigma^+$).[31,32] Pulsed photolysis of H_2O_2 at 308 nm was used to produce superthermal OH(X) radicals with relatively high velocities centred around 3500 ms^{-1}. After a short delay, a fraction of these superthermal OH(X) radicals are pumped on a specific A ← X transition to the electronically excited OH(A) state. The linear polarization of the dye laser pump pulse creates an initial rotational angular momentum alignment.

In general, for any molecule, the presence of magnetic field will lift the degeneracy of the m_j sublevels (*i.e.* the Zeeman splitting). In this case, a static, weak and homogeneous field (up to 10 G) was provided by a pair of Helmholtz coils (see Fig. 9). The dye laser in these experiments has a sufficiently broad frequency spectrum to excite a coherent superposition

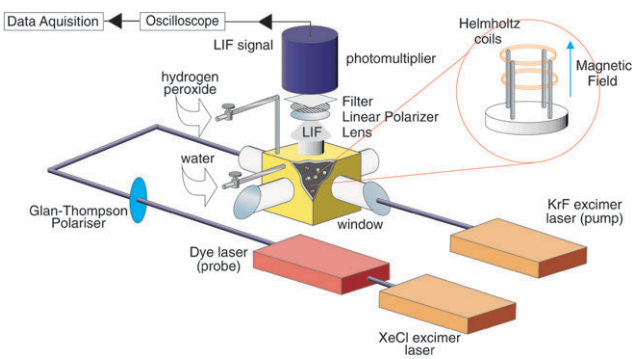

Fig. 9 Experimental apparatus used in the Zeeman quantum beat technique. The Helmholtz coils are shown schematically in the inset. Figure adapted with changes from ref. 32.

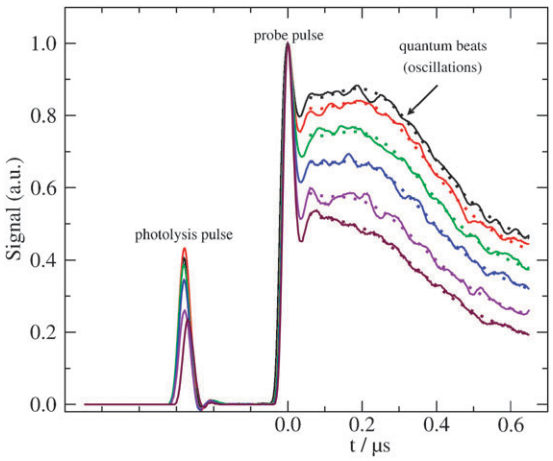

Fig. 10 Decay traces (solid lines) of LIF signal for OH(A, $\nu = 0$, $N' = 14$, $j' = 14.5$) generated subsequent to excitation of OH(X) on the $R_1(13.5)$ transition. Magnetic field 10 G. Upper trace: 2 mTorr of H_2O_2–H_2O. Lower traces: the effect of adding H_2O up to a maximum partial pressure of 39 mTorr. Fits to data (dotted lines) using eqn (3). (Adapted from ref. 31 with permission. Copyright 2005 Taylor & Francis).

of the Zeeman sublevels. At a greater level of detail, the H-atom in OH has a non-zero nuclear spin, $I = 1/2$. Therefore each rotational level of the OH(A) state is split, even in the absence of the external field, into two hyperfine states characterized by the grand total angular momentum, $\boldsymbol{F}$, with $\boldsymbol{F} = \boldsymbol{I} + \boldsymbol{j}$. Whether these sublevels are also excited coherently depends on the detailed properties of the dye laser pulse and the particular rotational state.

The electric vector of the laser light is chosen to be polarized perpendicular to the external magnetic field and to the fluorescence detection direction. Consequently, beat frequencies superimposed on the normal exponential decay were detected in the unresolved fluorescence emission (see Fig. 10). Collisions with a bath gas, in this case H_2O, affect the decay in two distinct ways. They remove population from the excited electronic state with a rate constant, k_n. They also alter either the magnitude or alignment of $\boldsymbol{j}$ within the excited electronic state, with rate constant k_p, causing a damping of the oscillations. The decay can be described by eqn (3):

$$I(H,t) = Ae^{-k_n t}[1 + Ce^{-k_p t}\sum_F \cos(2\omega_F t + \phi)] \qquad (3)$$

where the sum is over all of the quantum states involved, and ϕ is a phase factor. The Larmor precession frequency $\omega_F = \mu_B g_F H/\hbar$, depends on the field strength, H, the Bohr magneton, μ_B, and the rotational g-factor, g_F.

The phenomenological first-order rate constants k_n and k_p are, as expected, linearly dependent on the H_2O concentration, but in general also have a non-collisional contribution.[31] They can be written as $k_n = k_0 + k_1[H_2O]$ and $k_p = k_2 + k_3[H_2O]$, respectively. The rate constant k_0 is linked to the radiative lifetime of the OH(A) state and k_1 describes OH(A) collisional electronic quenching by H_2O. Non-collisional depolarization, included through k_2, was found to be effectively negligible in practice compared to the dominant effect of collisional depolarization, $k_3[H_2O]$, in the pressure range employed.

As configured without any dispersion of the fluorescence, k_3 does not distinguish between elastic (j-conserving) and inelastic (j-changing) depolarization. The corresponding cross sections, obtained using the known mean collision velocity, were 83 Å^2, 78 Å^2, and 14 Å^2 for the upper states of the $R_{22}(4)$, $P_{11}(9)$ and $R_{11}(13)$ transitions, respectively. The values are smaller than those measured previously in flames. Hence, under superthermal conditions, depolarization is apparently less efficient than RET. The implication is that j-changing transitions are not always accompanied by a loss of alignment.

The Zeeman quantum beat technique has also very recently been applied to compare the depolarization rates of other systems, including NO(A) + Ar.[33] As a distinct kinematic case from OH(A) + Ar, it should provide an insight into the separate roles of the PES and of mass-related momentum-transfer effects in controlling collisional depolarization.

Case study 5: Collisions of rotational-state selected OH(X) by polarization spectroscopy. Polarization Spectroscopy (PS) is a third-order non-linear spectroscopic technique, essentially a special case of the more general category of four-wave mixing.[34] It was originally developed as a variant of high-resolution saturation spectroscopy and subsequently used as an analytical tool in combustion research. It has recently been adapted by McKendrick and co-workers to measure collisional depolarization.[35] As shown schematically in Fig. 11, OH radicals are generated by 193 nm photolysis of HNO_3 in the presence of a bath of collider gas. Two independent dye laser systems, tuned to the same transition, are used to pump and probe the OH radicals on the $A^2\Sigma^+$–$X^2\Pi$ (0,0) band. The pump pulse has vertical linear polarization. The probe pulse is also linearly polarized, at 45° to the vertical. The pump pulse generates an alignment of the rotational angular momentum in the sample, in both the ground and excited states coupled by the transition. The probe pulse interacts with the polarized sample, generating a signal beam that co-propagates but has an orthogonal linear polarization. This signal beam is separated from the probe beam with a linear polarizer.

Crucially, any collisional process that removes the polarized sample will result in a loss of the PS signal. This includes j- (or fine-structure) changing collisions. These processes are measurable by other scalar methods as described in section 2.1. More interestingly, it also includes so-called elastic m_j-changing collisions that result in a change only in the plane, but not the classical speed, of rotation.

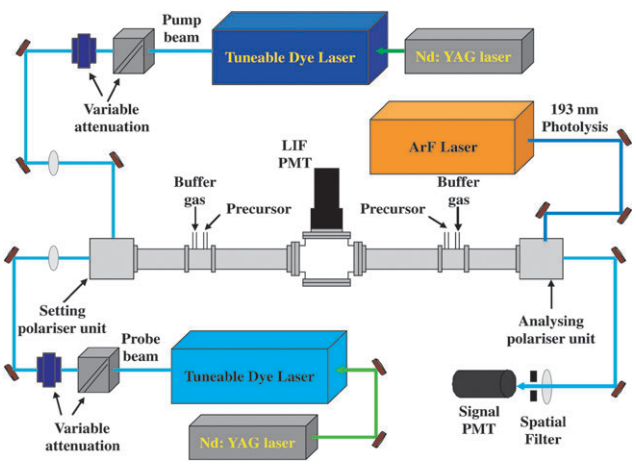

Fig. 11 Schematic diagram of the experimental apparatus used in the PS experiments of McKendrick and co-workers.

PS has been used by McKendrick and coworkers to study the loss of alignment of OH $X^2\Pi_{3/2}(j = 1.5–6.5, e)$ in collisions with He and Ar, using the $P_1(1.5)$–$P_1(6.5)$ transitions.[36] The rate of decay of the PS signal at a known collider pressure is measured by varying the delay between the pump and probe pulses. The decay rate *versus* collider pressure then provides second-order depolarization rate constants, k_{PS}. These are found to depend on j and collider gas, with Ar being consistently faster than He. No systematic trends are yet obvious in the j-dependence. To interpret these rate constants, the contribution of rotational, k_{RET}, and Λ-doublet, k_Λ, state-changing collisions was subtracted from k_{PS}, leaving the pure elastic m_j-changing rate constant, k_{DEP}. The state-changing rate constants were generated by QM scattering calculations on accurate *ab initio* PESs.[36] The results are shown in Fig. 12, where the total height of each bar is the measured k_{PS}, and the solid components are the theoretical rate constants k_{RET} and k_Λ. The unfilled section at the top of the bar therefore represents the desired, previously unknown, quantity k_{DEP}. Ar clearly causes much faster elastic depolarization than He. This is even more obvious if the rate constants are converted to thermally averaged collision cross-sections, with the result that typically $\sigma_{DEP}(Ar) \approx 5\sigma_{DEP}(He)$. This is in marked contrast to RET, where the total j-changing cross-sections for Ar are only slightly larger than for He.

These results can be related to the form of the PES for the two colliders. As discussed above, RET is largely determined by the anisotropy of the repulsive wall. Inspection of the PESs in Fig. 3 shows that OH–Ar and OH–He are similar in their repulsive form, with a modest reduction in radius for He. This is consistent with the observed RET rate constants (taking

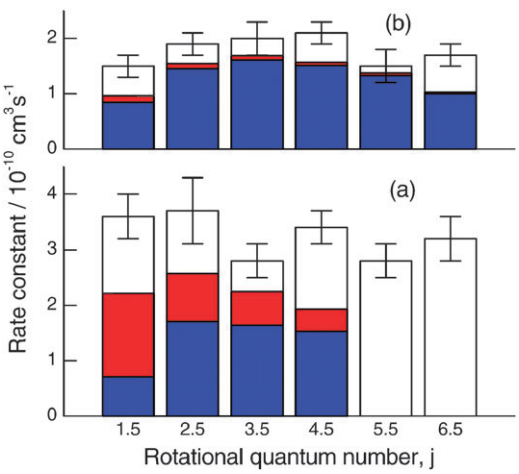

Fig. 12 Comparison of rate constants for PS signal loss, k_{PS} (white bars), with available corresponding theoretical values of RET, k_{RET} (blue bars), and Λ-doublet changing, k_Λ (red bars), rate constants. Collision partner (a) Ar and (b) He. The rate constants for elastic depolarization, k_{DEP}, can be obtained by subtracting the sum of k_{RET} and k_Λ from k_{PS}. (Adapted from ref. 36 with permission. Copyright 2007 PCCP Owner Societies).

account again of average thermal velocities). A short-range repulsive encounter is unlikely to change the plane of rotation without also causing RET. Indeed, in a classical model and within the limit of purely repulsive interactions, elastic depolarization does not occur. In contrast, the longer-range attractive parts of the PES can provide such a mechanism. Classically this can be viewed as the result of 'tumbling' collisions, where the collider approaches out of the plane of rotation, dragging the diatomic around as it passes through the attractive well.[37] OH–Ar has a much deeper and longer-range attractive potential than OH–He, as can be seen from Fig. 3. The depolarizing collisions detected by PS are thus sensitive to this difficult-to-observe part of the PES, which is not probed by conventional scalar RET measurements.

Case study 6: Collisions of velocity and rotational-state selected CN(X and A) by frequency-modulated spectroscopy. In recent years an all-optical method has been developed in reactive scattering studies to determine DCSs, the so-called 'photo-loc' method.[6] This method relies on the generation of a well-defined anisotropic velocity distribution of one reagent by polarized-laser photolysis of a suitable precursor. This fragment reacts with a thermalized bath of the other reagent, and the product velocity is measured by some laser-based spectroscopic technique. Provided the initial anisotropic collision velocity distribution is known, by applying the conservation of energy and linear momentum and some simple geometric relations, the measured product velocity may be used to determine the DCS.

This technique has recently been extended to the study of inelastic collision dynamics.[38] The experiment starts with the 266 nm photodissociation of ICN, to produce CN $X^2\Sigma^+$ ($v'' = 0, j''$), with a near mono-energetic and highly anisotropic velocity distribution. The collisional evolution of this anisotropic distribution can itself be investigated, but suffers from the disadvantage that the observed products are the cumulative result of collisions from the wide range of initial rotational states.[39] A much more powerful and incisive approach is to isolate a single initial quantum state. In the experiments of Alagappan *et al.*, the nascent CN $X^2\Sigma^+$ is optically pumped with a pulsed Nd:YAG/dye laser system, tuned to a chosen isolated transition in the $A^2\Pi$–$X^2\Sigma^+$ (4,0) band. Crucially, the pump-laser bandwidth and saturating pump conditions combine to ensure that the nascent CN velocity distribution is transferred without distortion to the chosen excited $A^2\Pi$ $v' = 4$ level. The result is an isolated quantum state (electronic, vibrational, rotational, spin–orbit and Λ-doublet specified) with a known velocity distribution. This is an ideal starting point for an inelastic scattering photo-loc experiment, which has now been successfully exploited with Ar as the selected collision partner.

The second challenge in a photo-loc experiment is the accurate measurement of the velocity distribution of the scattered products. This requires a quantum-state resolved spectroscopic technique with high sensitivity. Traditionally two techniques have been used, either REMPI-TOF/VMI (as described in case study 1) or sub-Doppler LIF. The first of these is limited to a few specific molecules by the viability of REMPI schemes in practice. LIF suffers from poor velocity resolution owing to the significant bandwidth of commercially available pulsed lasers. An alternative approach is to use continuous-wave probe lasers, for example the increasingly widely available external-cavity tuneable diode lasers. These have exceptionally narrow bandwidths, typically <10 MHz. This is very much less than the Doppler-broadened linewidths in a photo-loc experiment which are normally in the GHz range. The difficulty is that conventional absorption spectroscopy is relatively insensitive compared to LIF or ion-detection, and thus not suitable for probing the very low product number densities in a photo-loc experiment. This may be overcome by using a more sophisticated absorption method, in particular transient Frequency Modulated Spectroscopy (FMS). This is a high sensitivity, zero background technique. Its capability has been demonstrated recently through its successful application in the related field of photodissociation dynamics.[40] Sub-Doppler lineshapes are obtained by sweeping the laser frequency through a line.

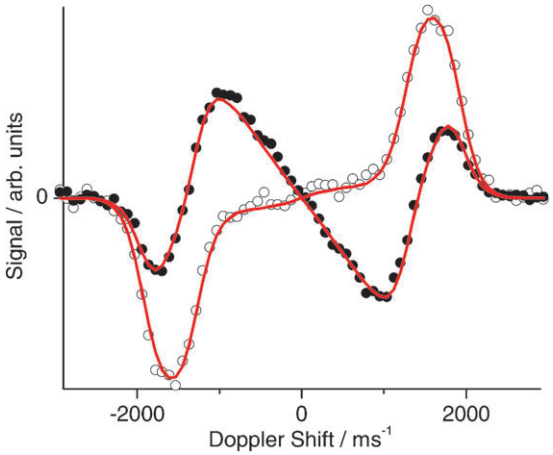

Fig. 13 Composite FM Doppler profiles dependent on the speed distribution (filled circles) and translation anisotropy (open circles) for CN $A^2\Pi_{1/2}$ ($v' = 4, j' = 0.5, f$) produced by collisions of ($j' = 1.5, e$) with Ar. The solid lines are the result of a fit to extract the DCS. (Adapted from ref. 38 with permission. Copyright 2007 American Institute of Physics).

In the experiments of Alagappan *et al.*, the scattered CN $A^2\Pi_{1/2}(v' = 4)$ was in fact probed by FMS in stimulated emission, which is entirely equivalent to absorption other than the sign of the signal. Fig. 13 shows FM Doppler profiles from probing the ($j' = 0.5, f$) product state on the A–X (4,2) band, where the initial population was pumped to the ($j' = 1.5, e$) state. The Doppler profiles are extracted from combinations of photolysis laser polarizations parallel and orthogonal to the probe laser propagation direction. Profiles are constructed that are sensitive to the speed and anisotropy of the angular distribution, respectively. The DCS derived from the fit in Fig. 13 is shown in Fig. 14, along with the corresponding DCSs for scattering from ($j' = 2.5, f$) and ($j' = 3.5, e$) into the same final state. These fully state-to-state resolved DCSs are all strongly forward scattered, as expected for small Δj transitions, but a clear trend to increasing sideways and backwards scattering is observed as Δj increases. For this relatively restricted range of scattered products it is not possible to determine whether the repulsive or attractive parts of the

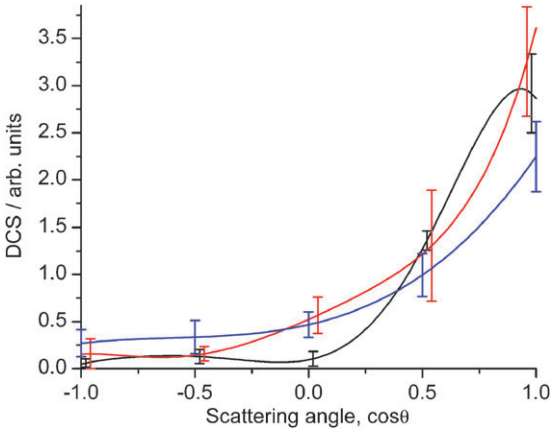

Fig. 14 DCSs for rotational energy transfer within the CN $A^2\Pi_{1/2}$ ($v' = 4$) manifold with Ar collider. Initial states ($j' = 1.5, e$) (black), ($j' = 2.5, f$) (red) and ($j' = 3.5, e$) (blue). Final state, ($j' = 0.5, f$), in all cases. (Adapted from ref. 38 with permission. Copyright 2007 American Institute of Physics).

PES are dominating the collision dynamics. However, these results, which are the first ever fully state-to-state resolved DCSs for RET in an electronically excited radical, do show the power of this experimental method. Unlike conventional molecular beam experiments, in principle any initial state may be selected. This evolving experiment is also expected to provide an independent test of the detailed predictions of QQT theory discussed in case study 2.

3. Conclusions and future prospects

We hope, through the case studies above, to have confirmed our proposition that significant new insights into the potential energy surfaces controlling collisional energy transfer are indeed being gained through the development of various novel 'vector' techniques. The power of some of these methods is now relatively well established. This category would include, for example, the crossed molecular beam/velocity map imaging approach in case study 1. Very detailed tests of both the repulsive and attractive parts of the PES were provided by the scattering angle-dependence of alignment and orientation, respectively, of NO colliding with Ar.

Others techniques are still at an earlier stage of their development, but nevertheless their principles have been demonstrated successfully and the prospect to yield more new and significant information in future unveiled. This might include Zeeman quantum beat spectroscopy of case study 4 and polarization spectroscopy of case study 5 as examples. These methods provide alternative novel probes of the extent to which the plane (and handedness) of rotation is preserved during collisions. The limited number of example systems examined so far indicate that these processes are sensitive to the long-range attractive parts of the PES. They therefore provide a valuable complement to scalar measurements of propensities in rotational energy transfer, which have been very widely observed to be dominated by the repulsive core of the PES. This has been the basis of the notable success of simple 'hard-sphere + hard-shape' and related models in interpreting RET results, for example in the linear-to-angular momentum conversion model developed by McCaffery.[41]

From a rigorous theoretical perspective, inelastic scattering was among the early problems to be treated by realistic QM scattering calculations when sufficient computational power first became available.[42] A number of propensities were predicted, or proposed and explored computationally through the accuracy of dynamical approximations.[43] Several of these were inherently vectorial, notably including the extent to which the plane of rotation (or, quantum mechanically, m_j) should be preserved during RET. As noted in section 2.1, these predictions have remained at best only sparsely tested in the meantime. The very limited number of collision systems that have been examined may not necessarily be typical, either kinematically or otherwise. Early examples, although ground-breaking, tended to be selected on the basis of experimental accessibility, such as I_2 with light partners, and BaO with Ar and CO_2.[44,45] The new experimental methods described above open up the possibility of a more extensive examination of such vector attributes of a greater range of systems, including the key radical species such as OH and NO that are important in combustion and the atmosphere. There is certainly scope for considerably more experimental work in this area. It is also to be hoped that the availability of these new data might stimulate renewed levels of theoretical interest, particularly since it is now possible to calculate what would be expected to be highly accurate PESs, including open-shell effects,[46] and perform scattering calculations on them.[47] The very directly 'stereochemical' nature of the experiments in case study 3, in which the molecular axis is oriented relative to the approach of the collision partner, certainly provide an intuitively particularly appealing test of this predictive ability. Case study 2 has also revealed that there may well be further undiscovered quantum propensities related to the electronic symmetries of the levels, and case study 3 has raised profound elementary questions such as even the direction of the dipole in NO. There are therefore a number of challenges that remain open to theory.

A future 'ultimate' experiment in this field might involve complete and arbitrary control over the initial internal states of the system, the polarization of the initial angular momentum and the relative collision velocity vector, coupled with corresponding state-specificity, angular momentum polarization and velocity detection of the products. This is arguably being approached in the 'photo-loc' experiments of case study 6. Obviously in practice there are real limitations on the degree of control that can be exerted. Nevertheless, it could represent an important advance towards this goal of measuring state- and polarization-specific differential cross-sections. One of the more important practical limitations is the extent of control of the collision energy through the photolysis wavelength used to generate the recoiling fragments, and its spread through the thermal motions of precursor and collisional target molecules. Greater control of the collision energy is being achieved through the latest molecular acceleration (and deceleration) techniques, which are just beginning to be applied to collisional energy transfer.[48] This potentially provides essentially continuous tunability of collision energies, including access to the new and almost entirely unexplored regime of 'ultracold' collisions.

Acknowledgements

We thank the EPSRC for relevant research grants, including postdoctoral research associate funding for SM and RCUK Academic Fellowship support for MLC. SM acknowledges support by the British Council and the Netherlands Organization for Scientific Research (NOW) for a research visit grant (PPS 883) and useful discussions with the groups of S. Stolte and M. Brouard on their experiments.

Notes and references

1 P. J. Dagdigian, in *Chemical Dynamics and Kinetics of Small Free Radicals*, ed. K. Liu and A. Wagner, World Science, Singapore, 1995, pp. 315–364.
2 P. J. Dagdigian, *Annu. Rev. Phys. Chem.*, 1997, **48**, 95.
3 A. J. McCaffery, M. J. Proctor and B. J. Whitaker, *Annu. Rev. Phys. Chem.*, 1986, **37**, 223.
4 A. Schiffman and D. W. Chandler, *Int. Rev. Phys. Chem.*, 1995, **14**, 371.
5 A. J. Alexander, M. Brouard, K. S. Kalogerakis and J. P. Simons, *Chem. Soc. Rev.*, 1998, **27**, 405.
6 M. Brouard, P. O'Keeffe and C. Vallance, *J. Phys. Chem. A*, 2002, **106**, 3629, and references cited therein.
7 A. J. Orr-Ewing and R. N. Zare, *Annu. Rev. Phys. Chem.*, 1994, **45**, 315.
8 G. Herzberg, *Molecular Spectra and Molecular Structure*, Vol. I—Spectra of Diatomic Molecules, Van Nostrand Reinhold, New York, 1950, pp. 218–237.
9 H.-S. Lee, A. B. McCoy, R. R. Toczyłowski and S. M. Cybulski, *J. Chem. Phys.*, 2000, **113**, 5736.
10 G. Paterson, S. Marinakis, M. L. Costen, K. G. McKendrick, J. Kłos and R. Tobola, manuscript in preparation.
11 W. R. Gentry, in *Atomic and Molecular Beam Methods*, ed. G. Scoles, Oxford University Press, Oxford, 1988, ch. 3, pp. 54–82.
12 J. C. Whitehead, *Rep. Prog. Phys.*, 1996, **59**, 993.
13 W. R. Gentry and C. F. Giese, *J. Chem. Phys.*, 1977, **67**, 5389.
14 P. A. Barrass, P. Sharkey and I. W. M. Smith, *Phys. Chem. Chem. Phys.*, 2003, **5**, 1400.
15 K. G. McKendrick, *J. Chem. Soc., Faraday Trans.*, 1998, **94**, 1921.
16 A. D. Rudert, J. Martin, W.-B. Gao, J. B. Halpern and H. Zacharias, *J. Chem. Phys.*, 1999, **111**, 9549.
17 A. D. Rudert, J. Martin, W.-B. Gao, H. Zacharias and J. B. Halpern, *J. Chem. Phys.*, 2000, **112**, 9749.
18 G. O. Sitz and R. L. Farrow, *J. Chem. Phys.*, 1994, **101**, 4682.
19 M. N. R. Ashfold, N. Hendrik Nahler, A. J. Orr-Ewing, O. P. J. Vieuxmaire, R. L. Toomes, T. N. Kitsopoulos, I. A. Garcia, D. A. Chestakov, S.-M. Wu and D. H. Parker, *Phys. Chem. Chem. Phys.*, 2006, **8**, 26.
20 K. Thomas Lorenz, D. W. Chandler, J. W. Barr, W. Chen, G. L. Barnes and J. I. Cline, *Science*, 2001, **293**, 2063.
21 E. A. Wade, K. Thomas Lorenz, D. W. Chandler, J. W. Barr, G. L. Barnes and J. I. Cline, *Chem. Phys.*, 2004, **301**, 261.
22 A. Gijsbertsen, H. Linnartz, G. Rus, A. E. Wiskerke, S. Stolte, D. W. Chandler and J. Kłos, *J. Chem. Phys.*, 2005, **123**, 224305.
23 A. Gijsbertsen, H. Linnartz and S. Stolte, *J. Chem. Phys.*, 2006, **125**, 133112.
24 A. Ballast, A. Gijsbertsen, H. Linnartz, C. A. Taatjes and S. Stolte, 25th International Symposium on Rarefied Gas Dynamics, St. Petersburg, American Institute of Physics, 2007, pp. 1263–1272.
25 A. Gijsbertsen, H. Linnartz, C. A. Taatjes and S. Stolte, *J. Am. Chem. Soc.*, 2006, **128**, 8777.
26 A. Gijsbertsen, H. Linnartz, J. Kłos and S. Stolte, *Phys. Scr.*, 2005, **72**, 1, and references cited therein.
27 C. A. Taatjes, A. Gijsbertsen, M. J. L. de Lange and S. Stolte, *J. Phys. Chem. A*, 2007, **111**, 7631.
28 A. Moise, D. H. Parker and J. J. ter Meulen, *J. Chem. Phys.*, 2007, **126**, 124302, and references cited therein.
29 M. C. van Beek, J. J. ter Meulen and M. H. Alexander, *J. Chem. Phys.*, 2000, **113**, 637.
30 M. H. Alexander and S. Stolte, *J. Chem. Phys.*, 2000, **112**, 8017.
31 M. Brouard, A. Bryant, I. Burak, S. Marinakis, F. Quadrini, I. A. Garcia and C. Vallance, *Mol. Phys.*, 2005, **103**, 1693.
32 S. Marinakis, *PhD thesis*, Linacre College, University of Oxford, 2005.
33 M. Brouard, personal communication, 2007.
34 S. Mukamel, *Principles of Nonlinear Optical Spectroscopy*, Oxford University Press, Oxford, 1995.
35 M. L. Costen, H. J. Crichton and K. G. McKendrick, *J. Chem. Phys.*, 2004, **120**, 7910.
36 S. Marinakis, G. Paterson, J. Kłos, M. L. Costen and K. G. McKendrick, *Phys. Chem. Chem. Phys.*, 2007, **9**, 4414.
37 H. R. Mayne and M. Keil, *J. Phys. Chem.*, 1984, **88**, 883.
38 A. Alagappan, I. Ballingall, M. L. Costen and K. G. McKendrick, *J. Chem. Phys.*, 2007, **126**, 041103.
39 A. Alagappan, M. L. Costen and K. G. McKendrick, *Spectrochim. Acta, Part A*, 2006, **63**, 910.
40 S. W. North and G. E. Hall, *Annu. Rev. Phys. Chem.*, 2000, **51**, 243.
41 A. J. McCaffery, *Phys. Chem. Chem. Phys.*, 2004, **6**, 1637.
42 D. Secrest, in *Atom-Molecule Collision Theory: A Guide for the Experimentalist*, ed. R. B. Bernstein, Plenum Press, New York, 1979, pp. 265–299.
43 V. Khare, D. J. Kouri and D. K. Hoffman, *J. Chem. Phys.*, 1981, **74**, 2275.
44 R. B. Kurzel and J. I. Steinfeld, *J. Chem. Phys.*, 1972, **56**, 5188.
45 S. J. Silvers, R. A. Gottscho and R. W. Field, *J. Chem. Phys.*, 1981, **74**, 6000.
46 J. Klos, M. M. Szczesniak and G. Chalasinski, *Int. Rev. Phys. Chem.*, 2004, **23**, 541.
47 F. J. Aoiz, J. E. Verdasco, V. J. Herrero, V. Sáez Rábanos and M. A. Alexander, *J. Chem. Phys.*, 2003, **119**, 5860.
48 J. J. Gilijamse, S. Hoekstra, S. Y. T. van der Meerakker, G. C. Groenenboom and G. Meijer, *Science*, 2006, **313**, 1617.